10 Jul 2023

Effect Of Internal Curing And Shrinkage-mitigating Materials On Microstructural Characteristics Of Fiber-reinforced Mortar

Kamran Aghaee

Kamal Khayat
Missouri University of Science and Technology, khayatk@mst.edu

Recommended Citation

K. Aghaee and K. Khayat, "Effect Of Internal Curing And Shrinkage-mitigating Materials On Microstructural Characteristics Of Fiber-reinforced Mortar," *Construction and Building Materials*, vol. 386, article no. 131527, Elsevier, Jul 2023.
The definitive version is available at https://doi.org/10.1016/j.conbuildmat.2023.131527

Construction and Building Materials 386 (2023) 131527

Contents lists available at ScienceDirect

Construction and Building Materials

journal homepage: www.elsevier.com/locate/conbuildmat

Effect of internal curing and shrinkage-mitigating materials on microstructural characteristics of fiber-reinforced mortar

Kamran Aghaee, Kamal H. Khayat *

Missouri University of Science and Technology, United States

ARTICLE INFO

Keywords:
Expansive agent
Interfacial transition zone
Lightweight sand
Microstructure
Shrinkage reducing admixture

ABSTRACT

Internal curing (IC) and other shrinkage mitigating materials are employed to reduce shrinkage and risk of cracking. This study investigates the efficiency of individual versus combined use of IC and shrinkage mitigating materials on key characteristics of fiber-reinforced mortar (FRM). The investigated mixtures include a 25% pre-saturated lightweight sand (LWS) that is added individually and combined with 10% CaO-based expansive agent (EA) and 2% shrinkage reducing admixture (SRA). This elucidates the synergistic effect of high content IC and EA/SRA on macro- and micro-mechanical characteristics of FRM, especially at the interface of the matrix with fibers. Mechanical properties, microstructural characteristics, and fiber–matrix bonding of FRM made with 0.5% steel fibers are investigated. The results show that the use of IC with EA and SRA completely compensates for shrinkage at 56 days. The highest compressive and fiber pull out strengths are observed for FRM with IC and without EA/SRA due to the densification of the interfacial transition zone (ITZ) confirmed by microstructural analysis. Such improvement is associated with the lower porosity of the cement paste and longer silicate chain—higher Si/Ca—obtained by FRM made with LWS. Although the combination of both EA and SRA with IC leads to 180 μstrain expansion after 56 days, the corresponding mixture presents the weakest ITZ and inferior mechanical properties.

1. Introduction

The development of high-performance concrete with low water-to-cementitious material ratio (w/cm), higher packing density, and low-permeability matrix has made the external curing water movement into depth of concrete less effective [1]. Internal curing (IC) as an effective curing technique has been successfully employed to reduce plastic, autogenous, and drying shrinkage and mitigate the risk of cracking [2–5]. IC can infuse water stored in pre-saturated lightweight aggregates (LWA) to increase the internal relative humidity of the hydrated cement paste. In order to achieve high surface area of LWA particles, enhance distribution in the cement paste to secure more uniform water dispersion throughout the hydrated cement paste, and to minimize the adverse effect of LWA on mechanical properties, the use of fine lightweight sand (LWS) is preferred [6–9]. Saturated LWS is usually made of expanded shale, clay, and slate is used to replace a given volume of natural sand to reduce self-desiccation. In 1991, Philleo [10] introduced the idea of using LWS as a promising solution to compensate for self-desiccation due to the hydration and chemical shrinkage in depth of concrete. The water in large capillary pores of LWS after cement hydration is drawn into the smaller cement paste pores to avoid self-desiccation and reduce autogenous shrinkage [7,11]. Trtik et al. reported that 3D images obtained by X-ray and neutron tomography for measuring water retention and migration throughout the matrix showed IC water in cement paste with a low w/cm of 0.25 was effective at least 3 mm into the cement paste after one day of age [12]. It is more common to use pre-saturated LWS, since LWS pores can otherwise be blocked in dry mixing, the use of dry LWS can make it difficult or impossible to saturate the LWS completely during concrete mixing. Additionally, the viscosity and surface tension of the pore solution due to less water injection into the pores can be increased by adding IC water into mixing water [13]. This phenomenon would lead to less effective shrinkage mitigation, as well as lower degree of hydration and mechanical properties. Golias et al. [13] reported that the substitution of 15% pre-saturated LWS with 24 h absorption of 17.5% can reduce the autogenous shrinkage of mortar with w/cm of 0.3 from −350 μstrain to a net expansion of +260 μstrain after one week of age. However, substituting 28% dry LWS (not pre-saturated) plus 0.06% additional IC water in the

* Corresponding author.
E-mail address: khayatk@mst.edu (K.H. Khayat).

https://doi.org/10.1016/j.conbuildmat.2023.131527
Received 11 August 2022; Received in revised form 19 February 2023; Accepted 22 April 2023
Available online 5 May 2023

Table 1
Physical and chemical characteristics of cement and Type G EA.

	OPC	EA
SiO_2, %	18.7	12.6
Al_2O_3, %	4.0	5.7
Fe_2O_3, %	3.6	1.9
CaO, %	65.9	82.6
MgO, %	1.7	0.1
SO_3, %	2.4	–
Na_2O eq., %	0.97	0.90
LOI, %	1.5	–
Blaine fineness, m^2/kg	390	–
Density, g/cm^3	3.14	3.12

Table 2
Characteristics of chemical admixtures.

Admixture	Solid content (%)	Specific gravity
HRWR	34.0	1.05
SRA	15.0	1.10

same mortar with similar effective w/cm degraded the IC performance and led to 50 μstrain lower expansion after a week.

Due to LWS pre-treatment requirements to ensure saturation, uncertainty of the uniform humidity, large scale of usage, and relatively quick water release, the use of super absorbent polymers (SAP) as an alternative IC material has recently drawn attention. SAPs are polymeric materials with ionic [14,15], non-ionic [14,16], and cationic [14,17] classifications, which were introduced by Jensen and Hansen in 2001 [15]. The use of SAP can also alleviate self-desiccation and shrinkage in cement-based materials [16,18]. The most common type of SAP for concrete IC is ionic with acrylic acid and cross-linked acrylamide-acrylic acid copolymer [16,18]. This type of SAP, due to their ionic and interconnected structure, absorb liquid up to 5000% of their mass [15,19] and desorb into the matrix gradually. The absorption/desorption kinetic is highly dependent on the physical and chemical characteristics of the SAP [14,20,21]. De Meyst et al. [22] reported that the use of 0.25% SAP with particle size (d_{50}) of 100 μm was more effective than that with 40 μm in shrinkage mitigation of cement paste with w/cm of 0.35, especially at early age. This can be justified by the smaller surface-to-volume ratio of the coarser SAP and its prompt IC water release versus the less active surface zone of the finer SAP and potential filling and blockage of particles with hydration products [15,22].

The effect of IC materials on mechanical properties and the quality of aggregate/fiber interfacial transition zone (ITZ) is controversial. Although the use of IC can promote cement hydration leading to densifying the hydrated cement paste [23,24], there is evidence that IC materials, depending on the utilized content, swelling rate, and generated porosity after water release, can diminish mechanical properties [18,25–28]. Santos et al. [29] studied the synergetic effect of using 1.3% steel fiber and up to 0.6% SAP. The authors reported that the use of 0.3% SAP can completely suppress autogenous shrinkage of high-performance concrete (HPC) from −425 μstrain shrinkage in the reference mixture to +40 μstrain expansion after 28 days with the lowest effect on compressive strength (16% reduction). The mechanical properties reduction can be due to the high absorption and swelling rate of the SAP particles, and the retained porosity after desorption of SAP particles.

In order to effectively limit shrinkage, shrinkage mitigating materials such as expansive agent (EA) and shrinkage reducing admixture (SRA) can be used in addition to IC [30]. The use of EA can partially compensate for drying shrinkage through an initial expansive reaction [31]. According to ACI 223 [32], EA can be classified in three categories: calcium sulfoaluminate (CSA)-, CaO-, and MgO-based that lead to the formation of expansive products, notably ettringite, $Ca(OH)_2$, and $Mg(OH)_2$ platelet crystals, respectively. Corinaldesi and Nardinocchi [33] reported that the coupled effect of 8% CaO-based EA and 2% hooked steel fibers in FRC can reduce the final shrinkage by 51% compared to the reference FRC mixture made without EA. The pre-stressing effect of fibers in the presence of EA was established as the reason for this enhancement.

SRA is a non-ionic surfactant that can reduce the surface tension of the water in capillary pores and maintains a higher internal relative humidity in the matrix, resulting in lower shrinkage [34]. Higher cracking resistance was exhibited when SRA was used in FRC, as well as cracking width limitation and time to cracking extension, even when half fiber content compared to the reference mixture was used [35]. The combination of shrinkage mitigating materials and IC can create large expansion which, if restricted by reinforcing bars and fibers, can induce internal stress and improve the mechanical properties and durability of concrete [36]. Wyrzykowski et al. [37] reported that the use of CSA-based EA, SRA, and SAP can lead to approximately 4000 μstrain expansion after 28 days of curing at 70% relative humidity. This expansion under restriction can induce 2.5–3 MPa chemical pre-stressing into the matrix. This can result in high compressive strength of around 100 MPa and superior durability.

The individual use of EA or SRA can compensate for shrinkage and their coupled use with IC can indeed amplify this effect [38–41]. For example, Li et al. [39] concluded that the combined use of 8% CaO-based EA and up to 10% pre-saturated LWS in concrete with 0.4 w/cm can increase the initial expansion by 60 μstrain and reduce the final shrinkage up to 50 μstrain compared to a mixture made with only EA. The coupled system limited the reduction in mechanical properties by single EA to 8%. The effect of combined shrinkage mitigating strategies on macro mechanical properties is relatively known [42–48]. However, their effect on microstructural characteristics and fiber–matrix interface characteristics especially at high content and combinations is unknown. Meticulous investigation to analyze the microstructure of the ITZ and understanding the mechanism of the binary and ternary combination of IC, EA, and SRA is needed. The current study utilized LWS content of 25% that is required to eliminate chemical shrinkage of the selected concrete [2,4,5,39,49] with and without EA/SRA, to maximize shrinkage reduction while exploring the effect on the aforementioned microstructural properties. In this regard, compressive strength development, fiber pull-out characteristics, and shrinkage of FRM mixtures (proportioned with w/cm of 0.4) were evaluated. Hydration kinetics, X-ray diffraction (XRD), thermo-gravimetric (TG), and scanning electron microscopy (SEM) analysis were employed to characterize the microstructure of the FRM matrix and the fiber–matrix ITZ.

2. Experimental program

2.1. Materials

A Type I/II ordinary portland cement (OPC), conforming to ASTM

Table 3
Mixture proportioning.

Mixture	OPC, kg/m^3	Sand, kg/m^3	EA, kg/m^3	SRA, kg/m^3	LWS, kg/m^3	Fiber, kg/m^3	HRWR, kg/m^3	Water, kg/m^3
25LWS	600	1103	0	0	253	39	1.8	239
25LWS10EA	540	1103	60	0	253	39	1.8	239
25LWS2SRA	600	1103	0	12	253	39	1.8	229
25LWS10EA2SRA	540	1103	60	12	253	39	1.8	229

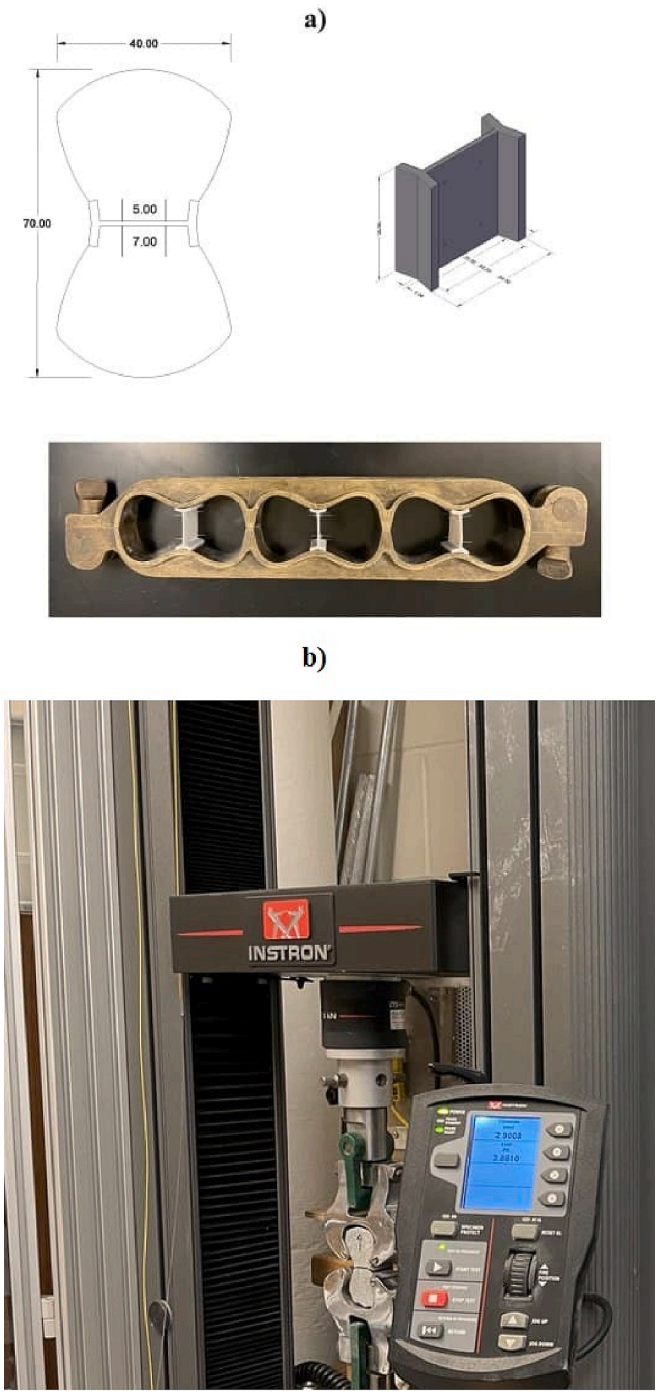

Fig. 1. (a) Schematic view of fiber pull-out sample, embedded plastic clip, and mold, (dimensions in mm); (b) fiber pull-out by Instron universal testing machine.

C150, was used. A CaO-based EA was utilized to compensate for shrinkage via initial expansion by the hydration of CaO. Table 1 presents the physical and chemical properties of the cement and EA.

Natural sand with fineness modulus of 2.6, specific gravity of 2.61, and saturated-surface-dry (SSD) water absorption of 0.36% was used in this study. Expanded shale LWS with SSD-specific gravity and absorption of 1.83 and 19%, respectively, was utilized for IC. Eq. (1) was applied to identify the required content of LWS:

$$M_{LWA} = \frac{C_f CS\alpha_{max}}{S\varnothing_{LWS}} \quad (1)$$

M_{LWA} is mass of dry LWS (kg/m^3), C_f is binder content (kg/m^3), and CS is chemical shrinkage of cement, which typically ranged between 0.06 and 0.08 for cementitious matrix made with OPC, at room temperature. In this study, CS of 0.08 was applied. α_{max} is the maximum expected degree of hydration (1), S is the degree of LWS saturation (1), and φ is absorption of LWS (19%) [50]. For measuring the absorption rate, the LWS was soaked in water for 72 h, and a 500-g sample was taken and spread on a thin layer on paper towel to dry by another paper towel until there was no shine on the aggregate surface or moisture absorbed by the paper towel. The weight of the sample was then recorded as W_{SSD}. The sample was allowed to dry in an oven at 105 °C for 24 h or until there was no change in weight. The oven dried weight was recorded as W_{OD}. The SSD absorption was calculated as follows:

$$Absorption = \frac{W_{SSD} - W_{OD}}{W_{SSD}} \times 100\% \quad (2)$$

Straight steel fibers measuring 13 mm in length and 0.2 mm in diameter (aspect ratio of 65) were used at 0.5% volumetric ratio. The modulus of elasticity and average tensile strength of the fibers were 200 GPa and 1200 MPa, respectively.

A polycarboxylate-based high-range water reducer (HRWR) at a constant ratio was utilized to achieve the required flowability. A shrinkage reducing admixture (SRA) was used to mitigate shrinkage by reducing the surface tension of the pore fluid. Considering 34% and 15% solid part associated with HRWR and SRA, 66% and 85% mass of HRWR and SRA were subtracted from the mixing water. The characteristics of the mentioned chemical admixtures are presented in Table 2.

2.2. Mixture proportioning

Table 3 presents the mixture proportioning of the four investigated FRM mixtures. The mixtures were prepared with 0.40 w/cm and a fixed HRWR dosage of 0.3% (active powder), by mass of binder. In order to achieve a superior shrinkage performance, the highest suggested amount of shrinkage mitigating materials was applied [30]. The EA and SRA contents corresponded to 10% and 2% of the binder mass, respectively. The LWS, which was pre-saturated for 72 h was replaced by 25% of the total volume of sand. All the mixtures were reinforced with 0.5% steel fiber. The nomenclature of each mixture refers to the amount of EA, SRA, and LWS (e.g., 10EA2SRA25LWS denotes an FRM mixture including 10% EA, 2% SRA, and 25% LWS, respectively).

2.3. Mixing and curing

Five-liter batches of FRM were prepared for each mixture using a Hobart mixer. The mixing procedure began with stirring the OPC and EA for one minute. Sand was then introduced and mixed for two minutes. The HRWR diluted in the mixing water was then added, and the mortar was mixed for three more minutes at 140 revolutions per minute (rpm). If SRA applied, it was included following the mixing water and HRWR and mixed for one minute. Subsequently, the mortar rested for two minutes. In the meantime, dog bone samples for the fiber pull-out testing were cast. Finally, the steel fibers were added, and the FRM was mixed at high speed of 285 rpm for two more minutes. Compressive strength and shrinkage samples were cast in one and two lifts, respectively. All the samples were consolidated using a vibrating table. After casting, the molds were covered with a damp burlap and plastic sheet to prevent moisture loss. Samples were demolded after 24 ± 1 h and stored in a lime-saturated water at 23 ± 2 °C until the age of 7 days. The shrinkage samples after demolding were covered with wet burlap and plastic sheet up to 7 days. Afterwards, all the samples were stored in lab with ambient temperature of 21 ± 3 °C and relative humidity of 50% ± 5%.

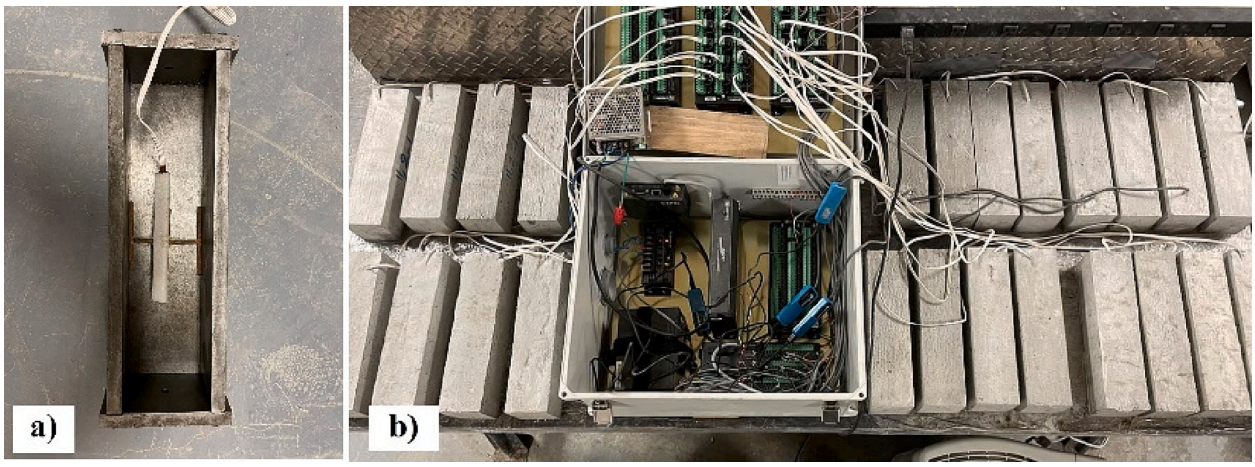

Fig. 2. (a) Shrinkage samples with 120 Ω embedded strain gauges located in the middle of mold; (b) strain gauges wired to DAQ.

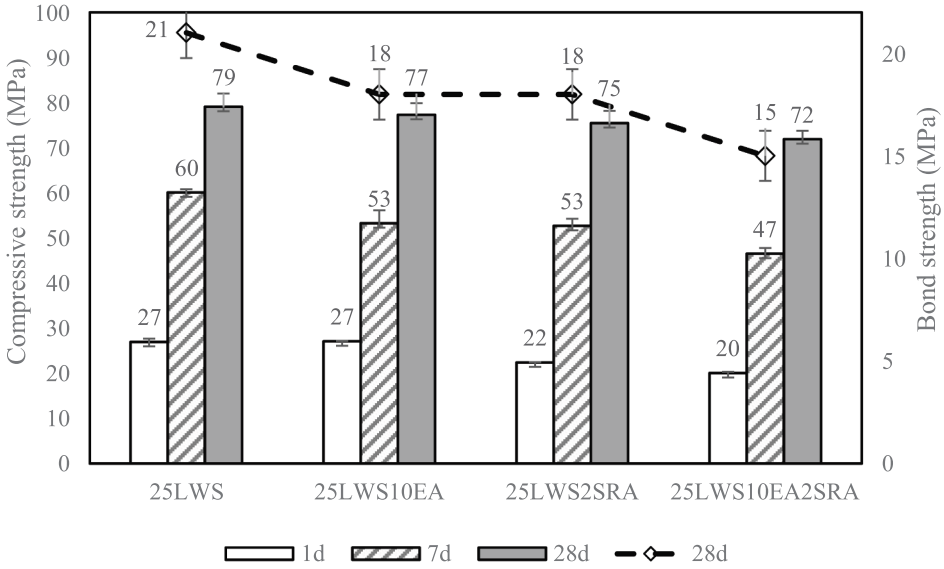

Fig. 3. Compressive strength development and fiber pull-out bond strength of investigated FRM mixtures.

Table 4
Fiber pull-out peak load and energy at 28 days.

Mixture	Peak Load (N)	Bond strength (MPa)	Energy (N.mm)
25LWS	173	21	85
25LWS10EA	151	18	72
25LWS2SRA	148	18	70
25LWS10EA2SRA	121	15	51

2.4. Testing methods

2.4.1. Compressive and fiber pull-out strength testing

Compressive strength testing was performed on FRM cubes of 50 × 50 × 50 mm, according to ASTM C109 [51]. Compressive strength samples were tested at 1, 7, and 28 days of age using a Tinius Olsen universal testing machine with loading rate of 0.9 kN/s and break detection of 50%. The reported strengths represent the average of at least three and maximum five FRM tested samples.

To evaluate the fiber–matrix bonding, fiber pull-out testing was performed on dog bone mortar samples (Fig. 1). Four steel fibers were perpendicularly inserted into the holes that were punched into a 3D printed plastic clip and evenly spaced at 15-mm spacing. The plastic clip was used to induce direct uniaxial tension only at the interaction of fiber–matrix. A shorter fiber development length of 5 mm was embedded into the pull-out half of the samples to ensure one side pull-out (Fig. 1). The fibers were fixed in the holes using super glue before casting the mortar. The samples were tested using an Instron universal testing machine with loading rate of 1 mm/min at the age of 28 days, according to CECS13-2009 [52] (Fig. 1b). The bond strength between the fibers and the matrix was calculated using Eq. (3).

$$\tau_{max} = \frac{P_{max}}{n\pi dl} \tag{3}$$

where, τ_{max} (MPa) is the bond strength between fibers and matrix at the maximum pull-out load; P_{max} (N) is the maximum pull-out load; n is the number of fibers (4); d (mm) is the diameter of a single fiber; and l (mm) is the embedment length of the fiber in pull-out half (5 mm). The pull-out energy (N.mm) was obtained by calculating the area under the load–displacement curve.

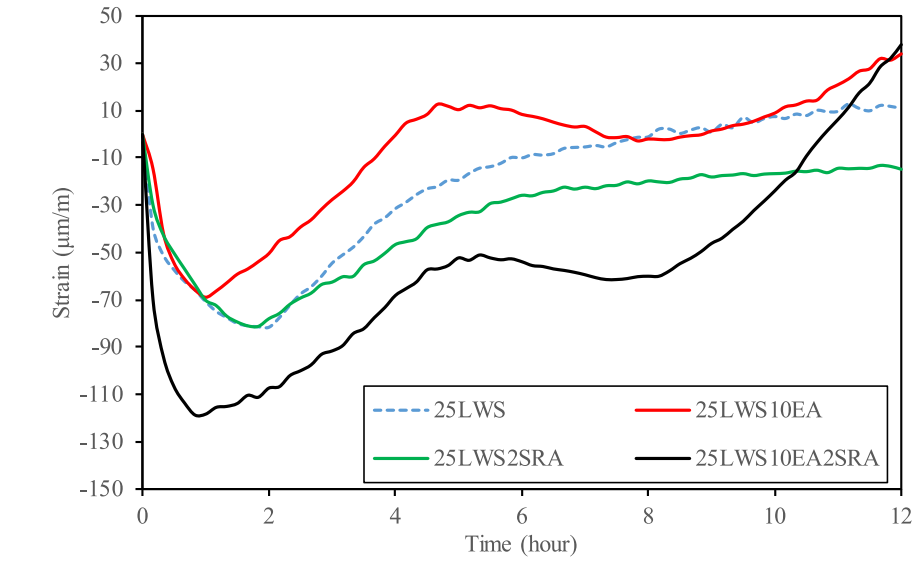

(a)

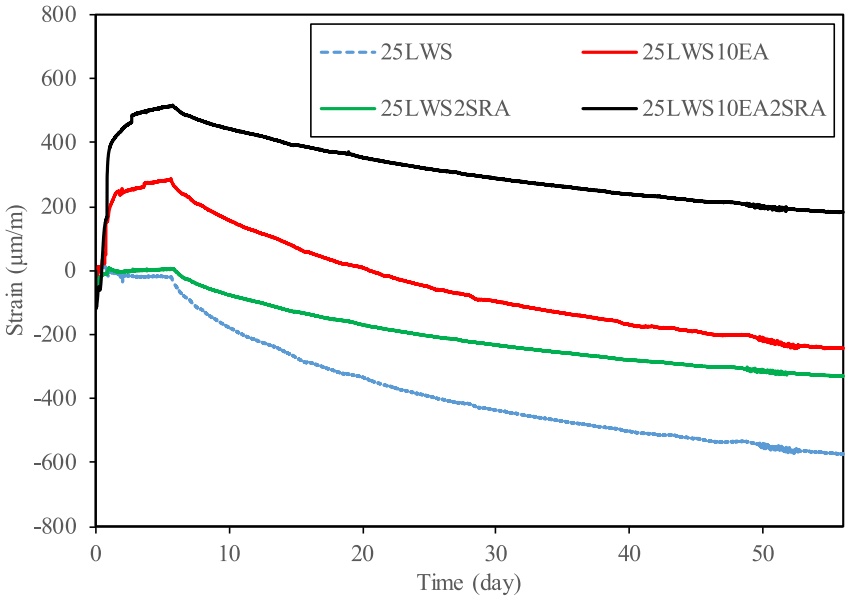

(b)

Fig. 4. (a) Early age shrinkage strain; (b) overall shrinkage strain of FRM mixtures.

Table 5
Cumulative heat of hydration for FRM mixtures over 48 h of hydration.

Mixture	Heat of hydration (J/g_{cement})		
	12 h	24 h	48 h
25LWS	88	189	249
25LWS10EA	103	209	267
25LWS2SRA	54	163	236
25LWS10EA2SRA	83	181	239

2.4.2. Shrinkage

Shrinkage testing was performed on 300 × 75 × 75 mm prismatic samples up to 56 days, as recommended by ASTM C157 [53]. Two samples were tested for each mixture. As Fig. 2a shows, for each sample a 120 Ω strain gauge with a gauge factor of 2.12 ± 0.5% was mounted on a chair in the middle of the mold. The strain gauges were wired up to the CR 1000 Campbell Scientific data acquisition system (DAQ) to collect the measurements immediately after casting the samples in 10-min intervals up to 56 days (Fig. 2b). This enabled the determination of the strain before and after setting for all the mixtures.

2.4.3. Hydration kinetics

Mortar samples were inserted into I-Cal 8000 isothermal calorimeter approximately after 10 min from water and cement contact. The calorimeter measured the rate and extent of heat release during the hydration of FRM mixtures, in compliance with ASTM C1679 [54]. It was programmed to maintain an isothermal condition at temperature of 20 °C for 48 h. Thermopiles converted the thermal flux to voltage and the data was recorded by a DAQ. Heat flow (mW/g_{cement}) and heat of hydration (J/g_{cement}) were calculated up to 48 h.

2.4.4. Internal relative humidity

In order to evaluate the effect of shrinkage mitigating materials on

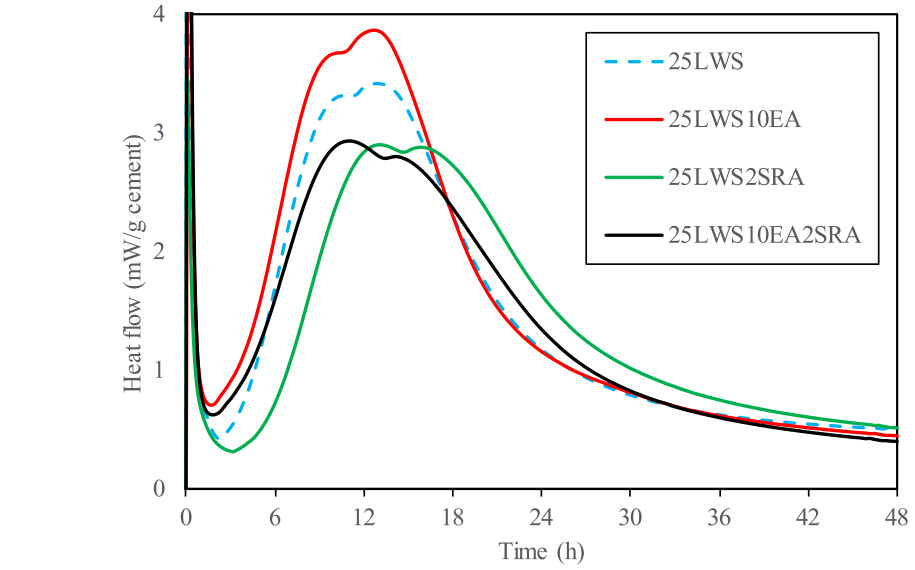

(a)

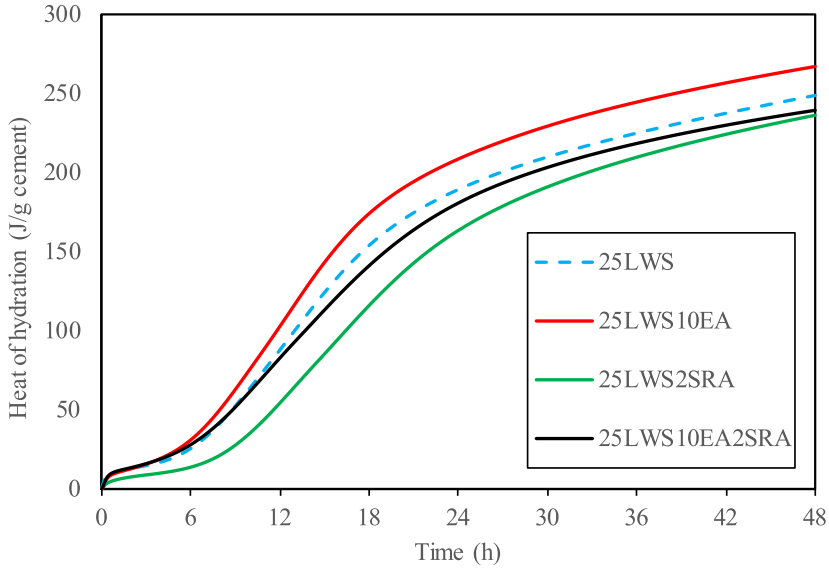

(b)

Fig. 5. (a) Heat flow; (b) cumulative heat evolution of FRM mixtures.

the internal relative humidity of FRM mixtures, USB-PTH450 sensors manufactured by Dracal Technologies were employed. The sensors were housed inside 10-mm diameter copper pipes sealed with silicon at the bottom and top, and embedded into the mixtures made with EA and SRA. Immediately after casting, the sensors were placed in one of the shrinkage prisms spaced evenly at 35 ± 5 mm from the sides of the prisms. Data was collected in one-minute intervals.

2.4.5. X-Ray diffraction (XRD)

FRM cubes similar to the compressive strength samples were cast for microstructure testing. The samples were crushed and soaked in isopropyl alcohol to stop hydration, after 28 days. Then, the samples were removed from alcohol and oven dried at 60 °C for 24 h. Up to 5 g of crushed particles were ground to powder. The ground powder was sieved through a 75 μm sieve before use. According to NBS SRM 674, as the internal standard 30 wt% anatase TiO_2 was added to each sample [55]. The XRD analysis was carried out using a Philips MPD X-ray diffractometer to characterize crystalline phases of FRM mixtures at 2θ values ranging from 5° to 90° and scanning rate of 1.5°/min. Rietveld refinement was performed using the analysis software (RIQAS) to find the peaks.

2.4.6. Thermo-gravimetric (TG) analysis

The TG analysis was implemented using a Netzsch Simultaneous instrument (Model 429) to quantitatively estimate the amount of hydration products of FRM mixtures. Hydration of the FRM samples was stopped at 28 days by soaking them in alcohol for two weeks. The samples were then vacuum dried at 60 °C for at least 24 h. Then they were ground, and about 0.05 g powder, which was passed through a 0.075 mm sieve, was taken for the TG test. The powder samples were subjected to heat ranging from 20 to 1000 °C at a heating rate of 10 °C/min in a nitrogen gas flow of 60 ml/min.

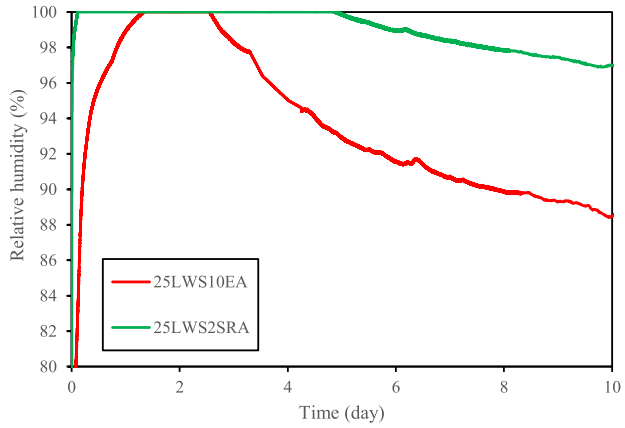

Fig. 6. Effect of shrinkage mitigating materials combination on relative humidity of FRM mixtures.

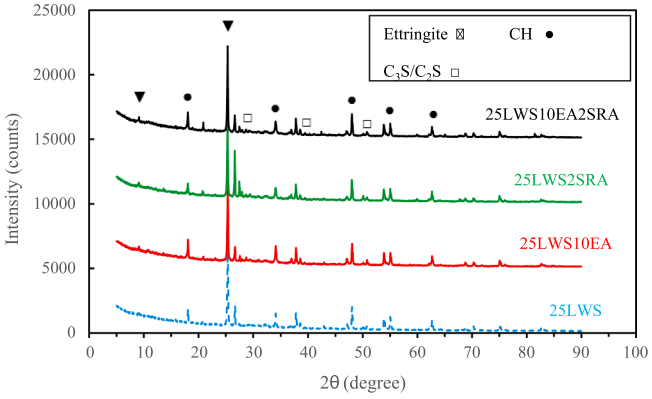

Fig. 7. XRD pattern of FRM mixtures at 28 days.

Table 6
Semi-quantitative analysis of crystalline phases for FRM mixtures at 28 days.

Mixture	Crystalline phase (%)		
	Ettringite	CH	C_3S/C_2S
25LWS	2.8	11.3	3.8
25LWS10EA	2.8	14.3	3.2
25LWS2SRA	3.5	10.3	3.7
25LWS10EA2SRA	3.0	12.1	3.0

2.4.7. Backscattered electron microscopy (BSEM)

The BSEM testing was conducted to investigate the microstructure features of the matrix and fiber–matrix interface, qualitatively and quantitatively. The chemical element mapping was used to determine the distribution of various elements at the fiber–matrix interface. An energy-dispersive spectrometry (EDS) using line scanning from the edge of fiber into 100 μm matrix was conducted to quantitatively evaluate element distribution and assess the fiber–matrix ITZ. The point scanning was employed to quantify the distribution of elements at the fiber–matrix interface and into the matrix.

For this test, samples measuring about 35 × 35 mm were cut using a diamond saw blade from intact 50 × 50 mm FRM cubes and dried overnight at 45 °C before mounting in epoxy. The samples were then soaked in epoxy. While the epoxy was still fluid, a vacuum was applied for about 10 min. Afterward, the samples were polished with 220 to 4000 grit pads, prior to the application of diamond paste as the final polish. After polishing, the samples were gold-coated using Denton desk V standard sputter coater. The BSEM testing was carried out using a Tescan VEGA3 scanning electron microscope with back-scattered detector in high vacuum mode.

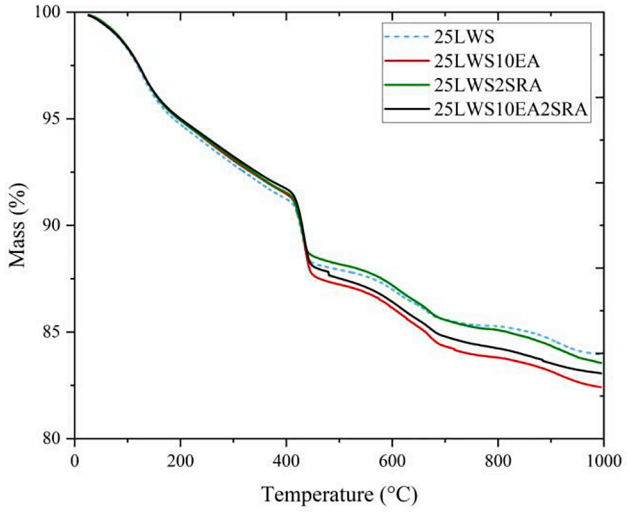

Fig. 8. Mass loss curves of FRM mixtures subjected to TG test.

3. Test results and discussion

3.1. Compressive and fiber pull-out strength

Fig. 3 shows the compressive strength of the investigated mixtures at 1, 7, and 28 days versus their bond strength at 28 days. It is shown that although there is not a significant compressive strength reduction resulting from the use of shrinkage mitigating materials in the presence of IC, the use of EA or SRA reduced the bonding strength with the embedded fibers by 14%. The individual use of 25% LWS resulted in the highest 28-day compressive strength (79 MPa) and bond strength (21 MPa). The use of EA and SRA in addition to IC resulted in insignificant (77 and 75 MPa, respectively) compressive strength reduction of FRM mixtures. The mixture made with the ternary combination of LWS, EA, and SRA exhibited the lowest 28-day compressive strength of 72 MPa and bond strength of 15 MPa. The compressive strength reduction was less than 10% compared to the 25LWS mixture, while the bonding strength was reduced by 28%. Comparing the effect of EA or SRA at the presence of IC (25LWS10EA or 25LWS2SRA mixtures) shows that the use of 10% EA did not change the initial strength development, while the incorporation of 2% SRA decelerated the compressive strength development compared to the 25LWS mixture. The use of EA coupled with LWS in the 25LWS10EA mixture improved the 1-day compressive strength by 23% compared to the 25LWS2SRA mixture. However, after 28 days similar strengths were recorded for both mixtures.

Table 4 presents the results of fiber pull-out testing on the investigated mixtures at 28 days. The highest peak load and pull-out energy was exhibited by the mixture made with 25% LWS. However, the lowest pull-out characteristics were demonstrated where the combined shrinkage mitigating strategy using all the shrinkage mitigating materials were utilized. The use of LWS with either EA or SRA (i.e., 25LWS10EA and 25LWS2SRA) diminished bond strength and pull-out energy by up to 14% and 18%, respectively. The use of LWS with both EA and SRA did not improve the fiber pull-out characteristics compared to the use of LWAS with EA/SRA (binary system). This can be due to the creation of internal microcracks resulting from an excessive initial expansion in the 10% EA mixture. Guo et al. [56] reported that the use of 10% CSA-based EA can reduce the fracture energy of concrete with compressive strength of 25 MPa and w/cm of 0.47. The excessive unrestrained expansion and the presence of microcracks are associated with the drop in fracture energy [56]. For the mixtures made with SRA,

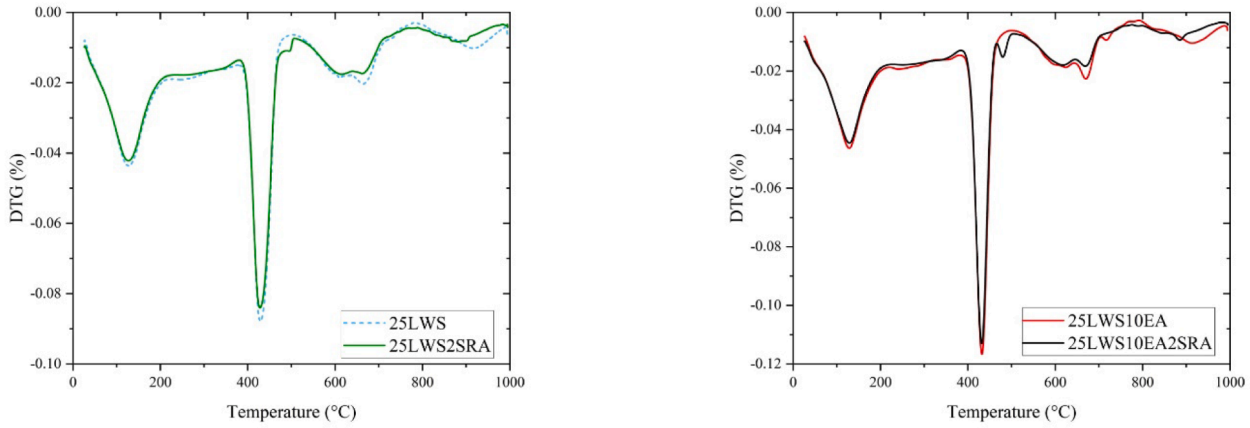

Fig. 9. Derivative thermogravimetric (DTG) curves of the (a) 25LWS vs. 25LWS2SRA and (b) 25LWS10EA vs. 25LWS10EA2SRA mixtures.

the reduction of radial confinement pressure at ITZ due to diminishing surface tension characteristics of SRA can contribute to lower fiber–matrix bonding strength. Yoo et al. [57] showed that the use of 2% SRA can reduce the average bond strength of fiber and matrix in ultra-high-performance fiber-reinforced concrete by 34% compared to the reference mixture made without SRA.

3.2. Shrinkage

Fig. 4a and b show early age shrinkage measured with strain gauges embedded in concrete up to 12 h and, overall shrinkage strain of the investigated mixtures up to 56 days, respectively. As seen in Fig. 4a, within the first two hours the lowest early age shrinkage was demonstrated by the 25LWS10EA mixture, while the highest was recorded for the 25LWS10EA2SRA mixture. However, after 12 h the combination of EA and SRA with LWS (25LWS10EA2SRA mixture) significantly compensated for the early age shrinkage and exhibited the same expansion as the 25LWS10EA mixture (30 μstrain).

As shown in Fig. 4b, after 56 days the highest expansion (+180 μstrain) and shrinkage (-570 μstrain) were recorded by the 25LWS10EA2SRA and 25LWS mixtures, respectively. Although higher initial expansion was demonstrated by using EA, the 25LWS10EA and 25LWS2SRA mixtures showed a mediocre strain range and converged at shrinkage strain of about −300 μstrain after 56 days. Corinaldesi [58] used 10% CaO-based EA and 1% SRA, by mass of cement, in a self-consolidating concrete. It was reported that the addition of EA was more effective than SRA in the initial expansion and final shrinkage compensation. The combination of EA and SRA caused stronger initial expansion, which gradually reduced while it remained positive after 60 days. Previous studies confirmed that higher EA expansion was obtained by the lower CH solubility. The presence of SRA can reduce the permittivity of water, and thus the water solubility of CH leading to higher expansion in the combined system of EA and SRA [59,60].

Considering Fig. 4b, although the overall shrinkage of the 25LWS mixture is highest (even more than 25LWS10EA2SRA mixture), yet as observed the mechanical properties of this mixture was the highest. Comparing the shrinkage and mechanical properties of these mixtures reveals that the initial expansion of the 25LWS10EA2SRA mortar occurs at early age when the matrix has not developed enough resistance to cracking, while the shrinkage of the 25LWS mixture gradually increased. In addition, the former mixture is subjected to a significant expansion followed by shrinkage, while the latter one experienced shrinkage only.

3.3. Hydration kinetics

Table 5 summarizes the cumulative heat of hydration for the investigated mixtures up to 48 h. The highest heat of hydration was obtained by the 25LWS10EA mixture, and the lowest was recorded for the 25LWS2SRA mixture. This justifies the prompt strength development of EA compared to SRA mixtures reported in Section 3.1. The effect of IC by the use of LWS combined with EA and SRA (25LWS10EA2SRA) on the heat of hydration was higher than that of the mixture made with SRA (25LWS2SRA), and lower than the one made with EA (25LWS10EA).

Comparing the heat of hydration and strength development of FRM mixtures, it can be realized that although the 25LWS10EA mixture showed the highest heat of hydration due to the reaction of CaO with water, the high expansion at early age and presence of microcracks in the matrix reduced strength development of the mixture, and as observed its early strength was equal to that of the 25LWS mixture. The incorporation of 2% SRA delayed cement hydration, while the presence of 10% EA in the 25LWS10EA2SRA mixture compensated for the net reduction in heat of hydration, and higher heat of hydration compared to the 25LWS2SRA mixture was recorded for the 25LWS10EA2SRA mixture. However, the presence of cracks due to the high expansion of the matrix led to lower strength compared to 25LWS2SRA mixture.

To better understand the effect of IC by LWS in the presence of EA/SRA on the performance of FRM, the heat evolution rate of FRM mixtures is plotted in Fig. 5a and b. It is shown that the 10EA mixtures exhibited the shortest induction period and highest peaks afterward. The enhanced heat evolution promoted portlandite (CH) generation and contributed to higher initial expansion of these mixtures, as observed in Section 3.3. The mentioned mixtures also presented a shorter acceleration/deceleration stage, which resulted in quick loss of the expansion. The longer induction period, low peak of heat flow, and relatively wide acceleration/deceleration stage presented by the 25LWS2SRA mixture explains the lowest cumulative heat of hydration, delayed strength development, and negligible expansion of this mixture, as discussed in sections 3.1 and 3.3. The effect of SRA on reducing the alkalinity of the pore solution, thus delaying, lowering, and widening the acceleration/deceleration peak, and reducing cumulative hydration hear release was reported in the literature [34,61,62].

3.4. Internal relative humidity

Fig. 6 shows the effect of the combination of EA and SRA on the

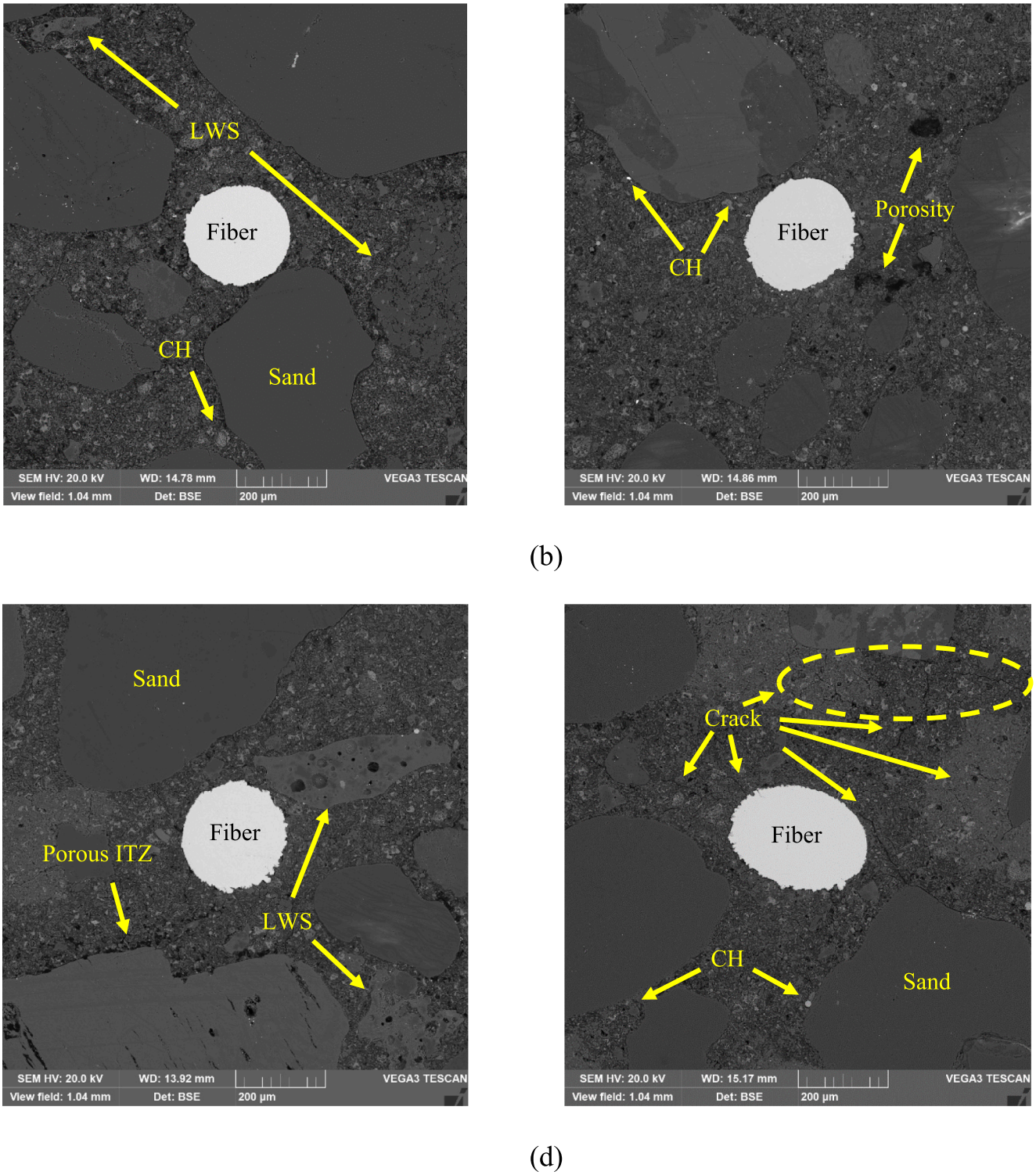

Fig. 10. BSEM images of (a) 25LWS, (b) 25LWS10EA, (c) 25LWS2SRA, and (d) 25LWS10EA2SRA mixtures at fiber–matrix interface at 28 days.

Table 7
Quantitative analysis of the chemical elements at the fiber–matrix interface.

Mixture	Element weight percentage								
	Fe	Ca	Mg	Si	Al	O	Na	K	C
25LWS	11.57	17.32	0.81	37.33	1.41	18.19	0.05	0.36	12.95
25LWS10EA	12.51	25.28	1.06	23.63	3.33	17.61	0.26	2.69	13.05
25LWS2SRA	11.38	19.68	0.90	27.63	3.64	17.14	0.25	5.99	13.17
25LWS10EA2SRA	13.44	24.18	0.97	29.60	1.60	17.88	0.16	1.53	10.65

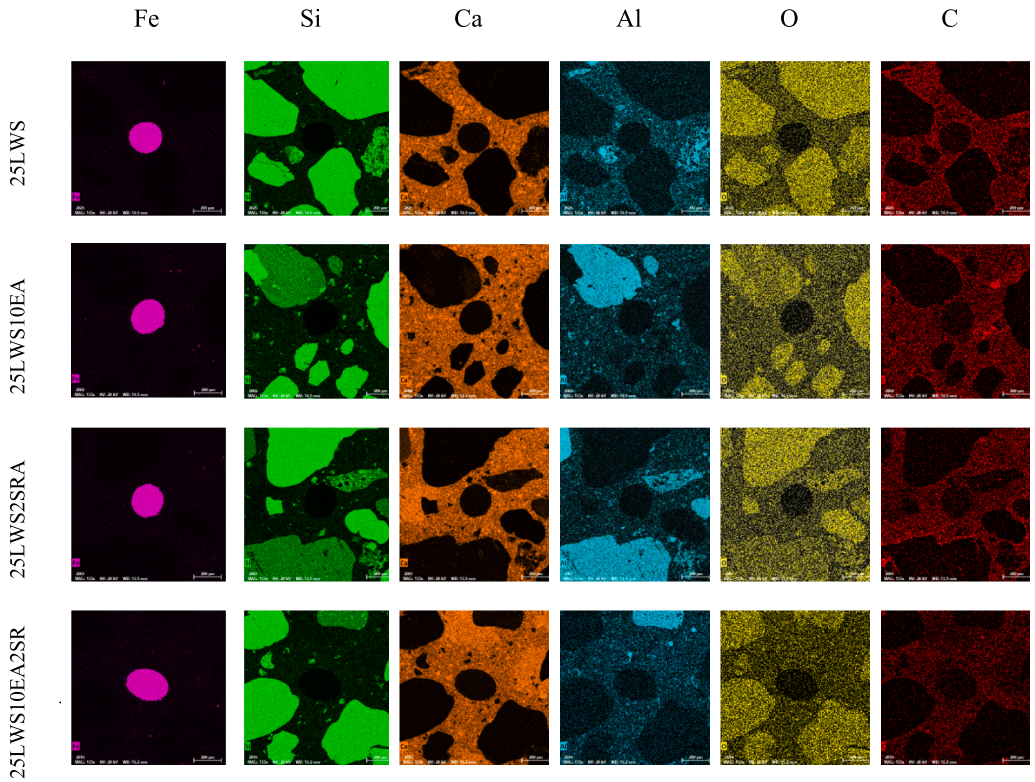

Fig. 11. Element-mapping of investigated mixtures at interface of fiber and matrix at 28 days.

relative humidity (RH) of FRM mixtures. As shown, the use of LWS coupled with SRA indicates extended 100% RH by the 25LWS2SRA mixture and a final RH of 95% after 10 days. However, the use of LWS coupled with EA resulted in lower RH in the first day due to the hydration of EA and formation of calcium hydroxide (CH). The water desorption by the LWS led to maintaining a temporary RH of 100% for a day and half, which dropped quickly to 88% after 10 days.

3.5. XRD analysis

Fig. 7 shows the XRD patterns, and Table 6 summarizes the semi-quantitative analysis of the crystalline phases of the investigated FRM mixtures at 28 days. Although during the crushing and grinding process, efforts were made to eliminate sand particles as much as possible, SiO_2 peaks were found in the XRD pattern, which were ignored in the semi-quantitative analysis of crystalline phases since they are not associated with a crystalline phase and are not formed by a chemical reaction. As shown in Fig. 7, the most prominent phase is CH with detected peaks at 2θ of 18°, 34°, 47°, and 55.5°. The higher intensity of CH peaks in the 25LWS10EA and 25LWS10EA2SRA mixtures confirm higher CH formation and expansion (Section 3.3) of these mixtures. The 25LWS2SRA mixture recorded the lowest amount of CH. The effect of SRA in hindering CH formation was reported in previous studies [60]. The peaks associated with ettringite formation were mostly found at 2θ of 8° and 25.5°. The unhydrated C_3S/C_2S peaked at 2θ of 29.3°, 39°, and 51.6°. Higher unhydrated binder were found for the 25LWS and 25LWS2SRA mixtures, compared to the 25LWS10EA and 25LWS10EA2SRA mixtures.

3.6. TG analysis

Fig. 8 illustrates the mass loss of the FRM mixtures that was determined using thermo-gravimetric (TG) analysis. The highest mass loss was associated with the mixtures containing 10% EA. This can justify the higher amount of water absorbed by EA for the formation of CH. The lowest mass loss was recorded for the 25LWS mixture, which presented the highest compressive strength and fiber pull-out bonding. Fig. 9a and b compare the results of derivative thermo-gravimetric (DTG) analysis for the FRM mixtures. All the mixtures exhibited the first major peak at around 160–170 °C, which was associated with the loss of chemically bound water into the C-S-H, ettringite, and monosulfate phases [63]. The C-S-H/ettringite formation of the 25LWS and 25LWS10EA mixtures are slightly higher than the 25LWS2SRA and 25LWS10EA2SRA mixtures. This indicates a higher C-S-H formation for the 25LWS and 25LWS10EA mixtures compared to the counterpart mixtures. The slightly higher C-S-H/ettringite formation can lead to stronger matrix and can correspond to the higher mechanical properties exhibited by the 25LWS and 25LWS10EA mixtures compared to 25LWS2SRA and 25LWS10EA2SRA mixtures (sections 3.1 and 3.2). The second peak, which appeared around 420 °C, corresponds to the decomposition of CH [64]. This peak refers to the CH consumption for the formation of C-S-H/ettringite and monosulfate phases. Although there is not much difference in the amount of CH by the mixtures shown in Fig. 9a and b, the higher presence of CH in the 25LWS and 25LWS10EA mixtures confirm the results obtained from the XRD analysis. The higher CH formation can enhance local indentation modulus and hardness of the mortar; however, the contribution to strength is not significant [65]. The last peaks at 600–700 °C and around 900 °C, which can be associated with the decarbonation of calcite [66], indicate insignificant carbonation that could occur during dry curing and sample preparation [67].

3.7. BSEM observation at fiber–matrix interface

BSEM images showing the microstructure of the investigated mixtures at the interface of fiber and matrix are presented in Fig. 10. The dark spots into the cement matrix indicate the presence of C-S-H, and brighter spots in these images represent the unhydrated grains. The amount of unhydrated grains due to the presence of LWS is not significant. This indicates that LWS provided adequate water to sustain greater cement hydration even in the presence of EA that reduces the internal RH. As shown in Fig. 10, the presence of CH deposited around voids and

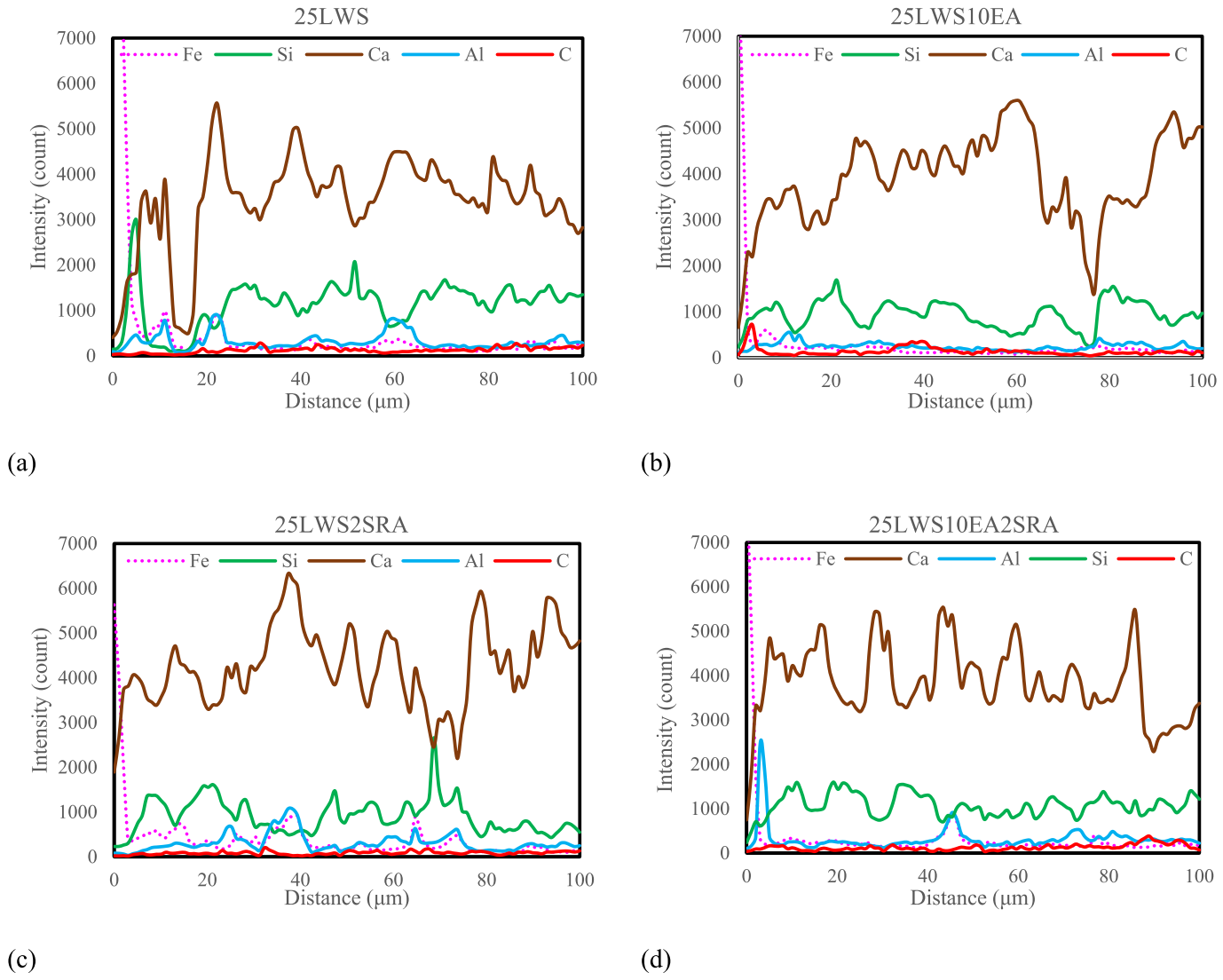

Fig. 12. Element distribution along scanning line at the interface of fiber for the (a) 25LWS, (b) 25LWS10EA, (c) 25LWS2SRA, and (d) 25LWS10EA2SRA mixtures.

at aggregate-matrix ITZ is visible in most of the mixtures. Fig. 10d shows the presence of major microcracking in the 25LWS10EA2SRA matrix. These cracks are not associated with sample preparation and testing condition, however, they can be due to the excessive initial expansion, as was reported in Section 3.3.

In the following sections, energy dispersive spectroscopy (EDS) electron scanning was utilized for surface scanning, chemical element mapping, line scanning, and point scanning at the fiber–matrix interface to analyze the characteristics of cement matrix and fiber–matrix ITZ. There were 10 to 15 fibers in each SEM sample. The SEM EDS surface/map/line scanning was performed on the ITZ regions of at least 10 fibers, and the common pattern for each mixture was identified and presented in this paper. The result of EDS point scanning was cumulatively presented for all 10 fibers in each sample/mixture.

3.7.1. *EDS surface scanning analysis*

The EDS was applied for scanning areas shown in Fig. 10 to identify the presence and content of various elements in the spectrums. Table 7 presents the quantitative analysis and elements weight percentage obtained by EDS surface scanning for the investigated mixtures. The higher content of Ca and Mg for the mixtures containing EA, 25LWS10EA, and 25LWS10EA2SRA confirms high content of CH, which agrees with the XRD analysis results. The high content of Si for the 25LWS mixtures contributes to the longer silicate chain and higher atomic ratio of Si/Ca, which causes a stronger C-S-H [68,69].

3.7.2. *EDS chemical element mapping analysis*

Fig. 11 displays element mapping at fiber–matrix interface, which provides the distribution of Fe, C, Ca, Si, Al, and O in the vicinity of fiber for the investigated mixtures. The pink area in the middle identifies steel fiber. The Si signifies sand particles and silicate in hydration products. The C can imply porosity. The other elements are representative of hydration products. The brighter spots refer to the greater and purer content of the element. Higher area showing Ca element for the 25LWS10EA and 25LWS10EA2SRA mixtures represents the higher content of CH due to the presence of EA in these mixtures.

3.7.3. *EDS line scanning analysis*

The EDS line scanning was applied to evaluate the variation in the characteristics of cement paste at the vicinity of the fiber. As previous studies have defined ITZ zone at around 50 to 100 μm of fiber, the chemical composition of the cement matrix within 100 μm of the fiber was investigated. In addition, the 100 μm distance for scanning was chosen since longer lines would interfere with sand particles. Fig. 12 shows the element distribution along selected scanning lines at the interface of fiber for the investigated mixtures. All the lines started from

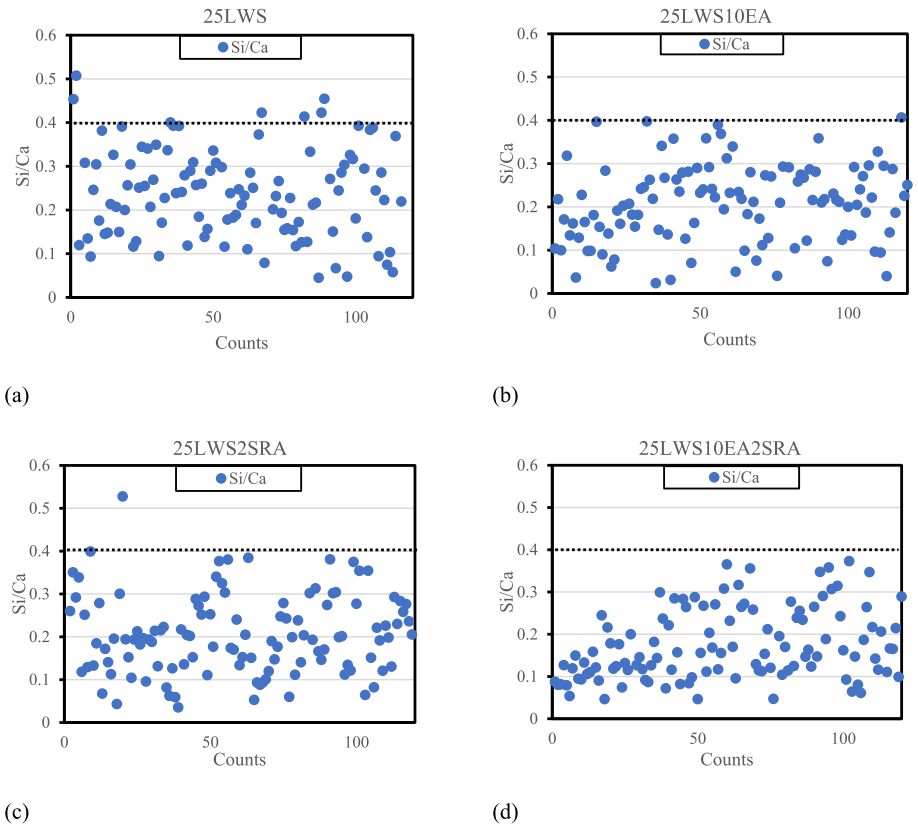

Fig. 13. Si/Ca ratio for the (a) 25LWS, (b) 25LWS10EA, (c) 25LWS2SRA, and (d) 25LWS10EA2SRA mixtures.

the edge of a fiber and passed through the matrix without any confliction with sand grains. This was the reason for a high intensity of Fe at the beginning of the plots and the absence of irregular Si bumps. As shown in Fig. 12, after the fiber zone the intensity of Fe significantly dropped and other elements such as Si, Ca, and Al dominated, signifying the cement matrix layer. In almost all the scanned lines the intensity of Ca is higher than Si, suggesting the presence of inner or outer C-S-H. The narrower gap between these elements for the 25LWS mixture indicates the higher C-S-H content and a stronger matrix. The higher Si to Ca intensity ratio can lead to longer silicate chain and enhance hardness and elastic modulus of C-S-H [70,71]. This characteristic, which is observed at the vicinity of the fiber in the 25LWS mixture, resulted in a stronger ITZ and higher fiber–matrix bonding as observed in Section 3.2.

The high intensity of C for the 25LWS10EA mixture, specially at the vicinity of the fiber, and relatively high intensity of C for the 25LWS10EA2SRA mixture between 80 and 100 μm indicates the high amount of porosity in these regions. This can imply the high expansion of these mixtures due to the use of 10% EA and the presence of micro-cracks into their matrix.

3.7.4. EDS point scanning analysis

In addition to porosity, phase assemblage of the hardened concrete plays a crucial role in the strength. The atomic ratio of Si/Ca for C-S-H can vary from 0.1 to 0.6 with the ratio of around 0.1 to 0.4 represent the outer C-S- H and 0.4 to 0.6 indicates inner C-S-H [72–74]. The inner C-S-H is denser with foil- or sheet-like morphology, and it forms on the surface of C_3S. However, the outer C-S-H is porous with fibrillar morphology, since it forms in the process of the dissolution of cementitious particles and formation of C-S-H intermixed with other phases such as CH, ettringite, and monosulfate [75,76]. The higher atomic ratio of Si/Ca contributes to longer silicate chain and higher strength [77–79]. To better understand the mechanism behind the strength development of the investigated mixtures, about 120 random points per sample at the vicinity of 10 fibers (around 200 μm)— fiber–matrix ITZ and matrix— with distances of about 50 μm were scanned, and their Si/Ca ratio was obtained by EDS point analysis. Sand particles and voids were avoided during scanning. Fig. 13 displays the Si/Ca of the scanned points for the investigated mixtures. As shown for the 25LWS mixture, more points associated with inner C-S-H or Si/Ca above 0.4 can be identified. For the 25LWS10EA and 25LWS2SRA mixtures, the majority of the scanned points are associated with outer C-S-H. There is not any point with Si/Ca of 0.4 or above for the 25LWS10EA2SRA mixture. This result is consistent with the mechanical properties of the investigated mixtures.

4. Conclusions

The effect of pre-saturated LWS on the performance of FRM mixtures prepared with and without EA and SRA was investigated. Compressive and fiber pullout strength, microstructure characteristics, and fiber–matrix interfacial bond of FRM reinforced with 0.5% steel fibers were evaluated. The following conclusions can be drawn:

1. The highest compressive strength and fiber pull out characteristics were exhibited by the mixture made with 25% LWS and without EA or SRA. This can be attributed to higher Si/Ca or higher content of inner C-S-H into the 25LWS mixture's matrix. The longer silicate chain at the vicinity of the fiber described the higher fiber pull out characteristics.
2. Although the use of EA/SRA resulted in slight reduction of mechanical properties, shrinkage was significantly improved with the coupled use of EA and SRA along with LWS. The 25LWS10EA and 25LWS10EA2SRA mixtures presented greater shrinkage compensation effects at 1 and 56 days.
3. The hydration kinetics, SEM, and TG analysis revealed high heat of hydration and CH formation in the 25LWS10EA and

25LWS10EA2SRA mixtures, leading to considerable initial expansion and greater degree of shrinkage compensation in the mentioned mixtures.

4. The BSEM observation and analysis confirmed a denser C-S-H (higher Si/Ca) at the vicinity of the fiber for the 25LWS mixture, and the presence of micro-cracks in the 25LWS10EA and 25LWS10EA2SRA mixtures due to the high content of EA.
5. The BSEM EDS point scanning at the vicinity of the fibers revealed that the Si/Ca ratio decreased with the use of EA/SRA. The high and low numbers of Si/Ca over 0.4 were recorded for the 25LWS and 25LWS10EA2SRA mixtures, respectively, confirming their observed mechanical properties.

CRediT authorship contribution statement

Kamran Aghaee: Conceptualization, Methodology, Data curation, Formal analysis, Validation, Visualization, Writing – original draft, Writing – review & editing. **Kamal H. Khayat:** Funding acquisition, Resources, Supervision, Writing – review & editing.

Declaration of Competing Interest

The authors declare that they have no known competing financial interests or personal relationships that could have appeared to influence the work reported in this paper.

Data availability

Data will be made available on request.

References

[1] R. Henkensiefken, D. Bentz, T. Nantung, J. Weiss, Volume change and cracking in internally cured mixtures made with saturated lightweight aggregate under sealed and unsealed conditions, Cem. Concr. Compos. 31 (7) (Aug. 2009) 427–437, https://doi.org/10.1016/j.cemconcomp.2009.04.003.

[2] M. Şahmaran, M. Lachemi, K.M.A. Hossain, V.C. Li, Internal curing of engineered cementitious composites for prevention of early age autogenous shrinkage cracking, Cem. Concr. Res. 39 (10) (Oct. 2009) 893–901, https://doi.org/10.1016/j.cemconres.2009.07.006.

[3] M.R. Geiker, D.P. Bentz, O.M. Jensen, Mitigating Autogenous Shrinkage by Internal Curing, SP 218 (Feb. 2004) 143–154, https://doi.org/10.14359/13060.

[4] W. Meng, K. Khayat, Effects of saturated lightweight sand content on key characteristics of ultra-high-performance concrete, Cem. Concr. Res. 101 (Nov. 2017) 46–54, https://doi.org/10.1016/j.cemconres.2017.08.018.

[5] A. Bentur, S. Igarashi, K. Kovler, Prevention of autogenous shrinkage in high-strength concrete by internal curing using wet lightweight aggregates, Cem. Concr. Res. 31 (11) (Nov. 2001) 1587–1591, https://doi.org/10.1016/S0008-8846(01)00608-1.

[6] R. Henkensiefken, J. Castro, H. Kim, D. P. Bentz, and J. Weiss, "Internal Curing Improves Concrete Performance throughout its Life," vol. 8, no. 5, pp. 22–30, Aug. 2009.

[7] D.P. Bentz, K.A. Snyder, Protected paste volume in concrete: Extension to internal curing using saturated lightweight fine aggregate, Cem. Concr. Res. 29 (11) (Nov. 1999) 1863–1867, https://doi.org/10.1016/S0008-8846(99)00178-7.

[8] J. Castro, L. Keiser, M. Golias, J. Weiss, Absorption and desorption properties of fine lightweight aggregate for application to internally cured concrete mixtures, Cem. Concr. Compos. 33 (10) (Nov. 2011) 1001–1008, https://doi.org/10.1016/j.cemconcomp.2011.07.006.

[9] M. Wyrzykowski, P. Lura, F. Pesavento, D. Gawin, Modeling of Water Migration during Internal Curing with Superabsorbent Polymers, J. Mater. Civ. Eng. 24 (8) (Aug. 2012) 1006–1016, https://doi.org/10.1061/(ASCE)MT.1943-5533.0000448.

[10] R. Philleo, Concrete Science and Reality, Mater. Sci. Concr. II (1991) 1–8.

[11] H. Chen, M. Wyrzykowski, K. Scrivener, P. Lura, Prediction of self-desiccation in low water-to-cement ratio pastes based on pore structure evolution, Cem. Concr. Res. 49 (Jul. 2013) 38–47, https://doi.org/10.1016/j.cemconres.2013.03.013.

[12] P. Trtik, B. Münch, W.J. Weiss, A. Kaestner, I. Jerjen, L. Josic, E. Lehmann, P. Lura, Release of internal curing water from lightweight aggregates in cement paste investigated by neutron and X-ray tomography, Nucl. Instrum. Methods Phys. Res., Sect. A 651 (1) (2011) 244–249.

[13] M. Golias, J. Castro, J. Weiss, The influence of the initial moisture content of lightweight aggregate on internal curing, Constr. Build. Mater. 35 (2012) 52–62.

[14] J. Liu, N. Farzadnia, K.H. Khayat, C. Shi, Effects of SAP characteristics on internal curing of UHPC matrix, Constr. Build. Mater. 280 (Apr. 2021), 122530, https://doi.org/10.1016/j.conbuildmat.2021.122530.

[15] O.M. Jensen, P.F. Hansen, Water-entrained cement-based materials: I. Principles and theoretical background, Cem. Concr. Res. 31 (4) (Apr. 2001) 647–654, https://doi.org/10.1016/S0008-8846(01)00463-X.

[16] V. Mechtcherine, H.-.-W. Reinhardt (Eds.), Application of Super Absorbent Polymers (SAP) in Concrete Construction: State-of-the-Art Report Prepared by Technical Committee 225-SAP, Springer, Netherlands, 2012, https://doi.org/10.1007/978-94-007-2733-5.

[17] C. Schröfl, K.A. Erk, W. Siriwatwechakul, M. Wyrzykowski, D. Snoeck, Recent progress in superabsorbent polymers for concrete, Cem. Concr. Res. 151 (Jan. 2022), 106648, https://doi.org/10.1016/j.cemconres.2021.106648.

[18] V. Mechtcherine, M. Wyrzykowski, C. Schröfl, D. Snoeck, P. Lura, N. De Belie, A. Mignon, S. Van Vlierberghe, A.J. Klemm, F.C.R. Almeida, J.R. Tenório Filho, W. P. Boshoff, H.-W. Reinhardt, S.-I. Igarashi, Application of super absorbent polymers (SAP) in concrete construction—update of RILEM state-of-the-art report, Mater. Struct. 54 (2) (2021), https://doi.org/10.1617/s11527-021-01668-z.

[19] V. Mechtcherine, M. Gorges, C. Schroefl, A. Assmann, W. Brameshuber, A. B. Ribeiro, D. Cusson, J. Custódio, E.F. da Silva, K. Ichimiya, S.-I. Igarashi, A. Klemm, K. Kovler, A.N. de Mendonça Lopes, P. Lura, V.T. Nguyen, H.-W. Reinhardt, R.D.T. Filho, J. Weiss, M. Wyrzykowski, G. Ye, S. Zhutovsky, Effect of internal curing by using superabsorbent polymers (SAP) on autogenous shrinkage and other properties of a high-performance fine-grained concrete: results of a RILEM round-robin test, Mater. Struct. 47 (3) (2014) 541–562.

[20] L. Senff, R.C.E. Modolo, G. Ascensão, D. Hotza, V.M. Ferreira, J.A. Labrincha, Development of mortars containing superabsorbent polymer, Constr. Build. Mater. 95 (Oct. 2015) 575–584, https://doi.org/10.1016/j.conbuildmat.2015.07.173.

[21] K. Farzanian, A. Ghahremaninezhad, Desorption of superabsorbent hydrogels with varied chemical compositions in cementitious materials, Mater. Struct. 51 (1) (Jan. 2018) 3, https://doi.org/10.1617/s11527-017-1128-1.

[22] L. De Meyst, E. Mannekens, K. Van Tittelboom, N. De Belie, The influence of superabsorbent polymers (SAPs) on autogenous shrinkage in cement paste, mortar and concrete, Constr. Build. Mater. 286 (Jun. 2021), 122948, https://doi.org/10.1016/j.conbuildmat.2021.122948.

[23] J. Yang, F. Wang, X. He, Y. Su, Pore structure of affected zone around saturated and large superabsorbent polymers in cement paste, Cem. Concr. Compos. 97 (2019) 54–67.

[24] J. Liu, N. Farzadnia, C. Shi, Effects of superabsorbent polymer on interfacial transition zone and mechanical properties of ultra-high performance concrete, Constr. Build. Mater. 231 (Jan. 2020), 117142, https://doi.org/10.1016/j.conbuildmat.2019.117142.

[25] A. Pourjavadi, S.M. Fakoorpoor, A. Khaloo, P. Hosseini, Improving the performance of cement-based composites containing superabsorbent polymers by utilization of nano-SiO2 particles, Mater. Des. 42 (Dec. 2012) 94–101, https://doi.org/10.1016/j.matdes.2012.05.030.

[26] S. Zhutovsky, K. Kovler, A. Bentur, Influence of cement paste matrix properties on the autogenous curing of high-performance concrete, Cem. Concr. Compos. 26 (5) (2004) 499–507.

[27] G. Lefever, E. Tsangouri, D. Snoeck, D.G. Aggelis, N. De Belie, S. Van Vlierberghe, D. Van Hemelrijck, Combined use of superabsorbent polymers and nanosilica for reduction of restrained shrinkage and strength compensation in cementitious mortars, Constr. Build. Mater. 251 (2020) 118966.

[28] Y. Wehbe, A. Ghahremaninezhad, Combined effect of shrinkage reducing admixtures (SRA) and superabsorbent polymers (SAP) on the autogenous shrinkage, hydration and properties of cementitious materials, Constr. Build. Mater. 138 (May 2017) 151–162, https://doi.org/10.1016/j.conbuildmat.2016.12.206.

[29] "Materials | Free Full-Text | Effect of the Combination of Superabsorbent Polymers for Autogenous Shrinkage Control with Steel Fibers of High-Performance Concrete under Uniaxial Tension Using DIC." https://www.mdpi.com/1996-1944/13/20/4638 (accessed Jan. 29, 2022).

[30] K. Aghaee, K.H. Khayat, Effect of shrinkage-mitigating materials on performance of fiber-reinforced concrete – An overview, Constr. Build. Mater. 305 (Oct. 2021), 124586, https://doi.org/10.1016/j.conbuildmat.2021.124586.

[31] P.K. Mehta, Mechanism of expansion associated with ettringite formation, Cem. Concr. Res. 3 (1) (Jan. 1973) 1–6, https://doi.org/10.1016/0008-8846(73)90056-2.

[32] "ACI 223-98 Standard Practice for the Use of Shrinkage- Compensating Concrete_ MyCivil.ir.pdf." https://1library.net/document/y44lpvky-aci-standard-practice-use-shrinkage-compensating-concrete-mycivil.html (accessed Jul. 01, 2021).

[33] V. Corinaldesi, A. Nardinocchi, Influence of type of fibers on the properties of high performance cement-based composites, Constr. Build. Mater. 107 (Mar. 2016) 321–331, https://doi.org/10.1016/j.conbuildmat.2016.01.024.

[34] F. Rajabipour, G. Sant, J. Weiss, Interactions between shrinkage reducing admixtures (SRA) and cement paste's pore solution, Cem. Concr. Res. 38 (5) (May 2008) 606–615, https://doi.org/10.1016/j.cemconres.2007.12.005.

[35] A. Passuello, G. Moriconi, S.P. Shah, Cracking behavior of concrete with shrinkage reducing admixtures and PVA fibers, Cem. Concr. Compos. 31 (10) (Nov. 2009) 699–704, https://doi.org/10.1016/j.cemconcomp.2009.08.004.

[36] K. Aghaee, N. Farzadnia, K.H. Khayat, Coupled effect of expansive agent and curing on mechanical and shrinkage properties of fiber-reinforced Eco-Crete, Constr. Build. Mater. 310 (Dec. 2021), 125285, https://doi.org/10.1016/j.conbuildmat.2021.125285.

[37] M. Wyrzykowski, G. Terrasi, P. Lura, Expansive high-performance concrete for chemical-prestress applications, Cem. Concr. Res. 107 (May 2018) 275–283, https://doi.org/10.1016/j.cemconres.2018.02.018.

[38] K. Aghaee, R. Sposito, K.H. Khayat, Synergistic effect of shrinkage mitigating materials on rheological properties of flowable and thixotropic cement paste, Cem. Concr. Compos. 133 (2022) 104686.
[39] M. Li, J. Liu, Q. Tian, Y. Wang, W. Xu, Efficacy of internal curing combined with expansive agent in mitigating shrinkage deformation of concrete under variable temperature condition, Constr. Build. Mater. 145 (Aug. 2017) 354–360, https://doi.org/10.1016/j.conbuildmat.2017.04.021.
[40] K. Aghaee, K.H. Khayat, Benefits and drawbacks of using multiple shrinkage mitigating strategies on performance of fiber-reinforced mortar, Cem. Concr. Compos. 133 (2022) 104714.
[41] K. Aghaee, R. Sposito, K.-C. Thienel, K.H. Khayat, Effect of additional water or superplasticizer on key characteristics of cement paste made with superabsorbent polymer and other shrinkage mitigating materials, Cem. Concr. Compos. 136 (Feb. 2023), 104893, https://doi.org/10.1016/j.cemconcomp.2022.104893.
[42] S. Anshuang, Q. Ling, Z. Shoujie, Z. Jiayang, L. Zhaoyu, Effects of Shrinkage Reducing Agent and Expansive Admixture on the Volume Deformation of Ultrahigh Performance Concrete, accessed Mar. 15, 2020, Adv. Mater. Sci. Eng. (2017), https://www.hindawi.com/journals/amse/2017/6384859/.
[43] S. Gao, Z. Wang, W. Wang, H. Qiu, Effect of shrinkage-reducing admixture and expansive agent on mechanical properties and drying shrinkage of Engineered Cementitious Composite (ECC), Constr. Build. Mater. 179 (Aug. 2018) 172–185, https://doi.org/10.1016/j.conbuildmat.2018.05.203.
[44] S. Zuo, Q. Yuan, T. Huang, M. Zhang, Q. Wu, Rheological behaviour of low-heat Portland cement paste with MgO-based expansive agent and shrinkage reducing admixture, Constr. Build. Mater. 304 (Oct. 2021), 124583, https://doi.org/10.1016/j.conbuildmat.2021.124583.
[45] M. Valipour, K.H. Khayat, Coupled effect of shrinkage-mitigating admixtures and saturated lightweight sand on shrinkage of UHPC for overlay applications, Constr. Build. Mater. 184 (Sep. 2018) 320–329, https://doi.org/10.1016/j.conbuildmat.2018.06.191.
[46] I. Mehdipour, K.H. Khayat, Enhancing the performance of calcium sulfoaluminate blended cements with shrinkage reducing admixture or lightweight sand, Cem. Concr. Compos. 87 (Mar. 2018) 29–43, https://doi.org/10.1016/j.cemconcomp.2017.12.001.
[47] J.-J. Park, D.-Y. Yoo, S.-W. Kim, Y.-S. Yoon, Drying shrinkage cracking characteristics of ultra-high-performance fibre reinforced concrete with expansive and shrinkage reducing agents, Mag. Concr. Res. 65 (4) (Feb. 2013) 248–256, https://doi.org/10.1680/macr.12.00069.
[48] D.-Y. Yoo, J.-J. Park, S.-W. Kim, Y.-S. Yoon, Combined effect of expansive and shrinkage-reducing admixtures on the properties of ultra high performance fiber-reinforced concrete, J. Compos. Mater. 48 (16) (Jul. 2014) 1981–1991, https://doi.org/10.1177/0021998313493809.
[49] R. Henkensiefken, P. Briatka, D. P. Bentz, T. Nantung, and J. Weiss, "Plastic Shrinkage Cracking in Internally Cured Mixtures Made with Pre-wetted Lightweight Aggregate," vol. 32, no. 2, pp. 49–54, Feb. 2010.
[50] P. Lura and J. W. Roberts, "Mixture Proportioning for Internal Curing," vol. 27, no. No. 2, pp. 35–40, Feb. 2005.
[51] A. C. ASTM C109/C109M-20, *Standard Test Method for Compressive Strength of Hydraulic Cement Mortars (Using 2-in. or [50-mm] Cube Specimens)*. ASTM International, West Conshohocken, PA.
[52] Z. Wu, K.H. Khayat, C. Shi, B.F. Tutikian, Q. Chen, Mechanisms underlying the strength enhancement of UHPC modified with nano-SiO2 and nano-CaCO3, Cem. Concr. Compos. 119 (May 2021), 103992, https://doi.org/10.1016/j.cemconcomp.2021.103992.
[53] ASTM C157, "Test Method for Length Change of Hardened Hydraulic-Cement Mortar and Concrete," ASTM International, 2017. doi: 10.1520/C0157_C0157M-17.
[54] "ASTM-C1679 | Standard Practice for Measuring Hydration Kinetics of Hydraulic Cementitious Mixtures Using Isothermal Calorimetry | Document Center, Inc." https://www.document-center.com/standards/show/ASTM-C1679/history/2009%20EDITION (accessed Mar. 22, 2022).
[55] National Institute of Standards & Technology, *Standard Reference Material 674b*. 2017.
[56] J. Guo, S. Zhang, T. Guo, P. Zhang, Effects of UEA and MgO expansive agents on fracture properties of concrete, Constr. Build. Mater. 263 (Dec. 2020), 120245, https://doi.org/10.1016/j.conbuildmat.2020.120245.
[57] D.-Y. Yoo, J. Kim, G. Zi, Y.-S. Yoon, Effect of shrinkage-reducing admixture on biaxial flexural behavior of ultra-high-performance fiber-reinforced concrete, Constr. Build. Mater. 89 (Aug. 2015) 67–75, https://doi.org/10.1016/j.conbuildmat.2015.04.040.
[58] V. Corinaldesi, Combined effect of expansive, shrinkage reducing and hydrophobic admixtures for durable self compacting concrete, Constr. Build. Mater. 36 (Nov. 2012) 758–764, https://doi.org/10.1016/j.conbuildmat.2012.04.129.
[59] S. Chatterji, Mechanism of expansion of concrete due to the presence of dead-burnt CaO and MgO, Cem. Concr. Res. 25 (1) (Jan. 1995) 51–56, https://doi.org/10.1016/0008-8846(94)00111-B.
[60] C. Maltese, C. Pistolesi, A. Lolli, A. Bravo, T. Cerulli, D. Salvioni, Combined effect of expansive and shrinkage reducing admixtures to obtain stable and durable mortars, Cem. Concr. Res. 35 (12) (Dec. 2005) 2244–2251, https://doi.org/10.1016/j.cemconres.2004.11.021.
[61] V. Bílek, L. Kalina, R. Novotný, J. Tkacz, L. Pařízek, Some Issues of Shrinkage-Reducing Admixtures Application in Alkali-Activated Slag Systems, Materials (Basel) 9 (6) (Jun. 2016) 462, https://doi.org/10.3390/ma9060462.
[62] J. Saliba, E. Rozière, F. Grondin, A. Loukili, Influence of shrinkage-reducing admixtures on plastic and long-term shrinkage, Cem. Concr. Compos. 33 (2) (Feb. 2011) 209–217, https://doi.org/10.1016/j.cemconcomp.2010.10.006.
[63] K. De Weerdt, M.B. Haha, G. Le Saout, K.O. Kjellsen, H. Justnes, B. Lothenbach, Hydration mechanisms of ternary Portland cements containing limestone powder and fly ash, Cem. Concr. Res. 41 (3) (Mar. 2011) 279–291, https://doi.org/10.1016/j.cemconres.2010.11.014.
[64] P. Hou, K. Wang, J. Qian, S. Kawashima, D. Kong, S.P. Shah, Effects of colloidal nanoSiO2 on fly ash hydration, Cem. Concr. Compos. 34 (10) (Nov. 2012) 1095–1103, https://doi.org/10.1016/j.cemconcomp.2012.06.013.
[65] J.J. Chen, L. Sorelli, M. Vandamme, F.-J. Ulm, G. Chanvillard, A Coupled Nanoindentation/SEM-EDS Study on Low Water/Cement Ratio Portland Cement Paste: Evidence for C-S–H/Ca(OH)2 Nanocomposites, J. Am. Ceram. Soc. 93 (5) (2010) 1484–1493, https://doi.org/10.1111/j.1551-2916.2009.03599.x.
[66] W. Wongkeo, P. Thongsanitgarn, P. Chindaprasirt, A. Chaipanich, Thermogravimetry of ternary cement blends, J. Therm. Anal. Calorim. 113 (3) (Sep. 2013) 1079–1090, https://doi.org/10.1007/s10973-013-3017-3.
[67] A.S. Silva, A. Gameiro, J. Grilo, R. Veiga, A. Velosa, Long-term behavior of lime–metakaolin pastes at ambient temperature and humid curing condition, Appl. Clay Sci. 88–89 (Feb. 2014) 49–55, https://doi.org/10.1016/j.clay.2013.12.016.
[68] B. Lothenbach, A. Nonat, Calcium silicate hydrates: Solid and liquid phase composition, Cem. Concr. Res. 78 (2015) 57–70.
[69] Y. Yan, S.-Y. Yang, G.D. Miron, I.E. Collings, E. L'Hôpital, J. Skibsted, F. Winnefeld, K. Scrivener, B. Lothenbach, Effect of alkali hydroxide on calcium silicate hydrate (C-S-H), Cem. Concr. Res. 151 (2022) 106636.
[70] J.J. Chen, J.J. Thomas, H.F.W. Taylor, H.M. Jennings, Solubility and structure of calcium silicate hydrate, Cem. Concr. Res. 34 (9) (Sep. 2004) 1499–1519, https://doi.org/10.1016/j.cemconres.2004.04.034.
[71] B. Lothenbach, K. Scrivener, R.D. Hooton, Supplementary cementitious materials, Cem. Concr. Res. 41 (12) (Dec. 2011) 1244–1256, https://doi.org/10.1016/j.cemconres.2010.12.001.
[72] A. Cuesta, J.D. Zea-Garcia, D. Londono-Zuluaga, A.G. De la Torre, I. Santacruz, O. Vallcorba, M. Dapiaggi, S.G. Sanfélix, M.A.G. Aranda, Multiscale understanding of tricalcium silicate hydration reactions, Sci. Rep. 8 (1) (Jun. 2018), https://doi.org/10.1038/s41598-018-26943-y.
[73] W. Kunther, S. Ferreiro, J. Skibsted, Influence of the Ca/Si ratio on the compressive strength of cementitious calcium–silicate–hydrate binders, J. Mater. Chem. A 5 (33) (Aug. 2017) 17401–17412, https://doi.org/10.1039/C7TA06104H.
[74] I.G. Richardson, The nature of the hydration products in hardened cement pastes, Cem. Concr. Compos. 22 (2) (Apr. 2000) 97–113, https://doi.org/10.1016/S0958-9465(99)00036-0.
[75] I.G. Richardson, The calcium silicate hydrates, Cem. Concr. Res. 38 (2) (Feb. 2008) 137–158, https://doi.org/10.1016/j.cemconres.2007.11.005.
[76] C. Famy, K.L. Scrivener, A. Atkinson, A.R. Brough, Effects of an early or a late heat treatment on the microstructure and composition of inner C-S-H products of Portland cement mortars, Cem. Concr. Res. 32 (2) (Feb. 2002) 269–278, https://doi.org/10.1016/S0008-8846(01)00670-6.
[77] F. Pelisser, P.J.P. Gleize, A. Mikowski, Effect of the Ca/Si Molar Ratio on the Micro/nanomechanical Properties of Synthetic C-S-H Measured by Nanoindentation, J. Phys. Chem. C 116 (32) (Aug. 2012) 17219–17227, https://doi.org/10.1021/jp302240c.
[78] J. Li, Q. Yu, H. Huang, S. Yin, Effects of Ca/Si Ratio, Aluminum and Magnesium on the Carbonation Behavior of Calcium Silicate Hydrate, Materials (Basel) 12 (8) (Apr. 2019) 1268, https://doi.org/10.3390/ma12081268.
[79] A. Babaahmadi, A. Machner, W. Kunther, J. Figueira, P. Hemstad, K. De Weerdt, Chloride binding in Portland composite cements containing metakaolin and silica fume, Cem. Concr. Res. 161 (Nov. 2022), 106924, https://doi.org/10.1016/j.cemconres.2022.106924.